An improved model for droplet solidification on a flat surface

J.-P. DELPLANQUE, R. H. RANGEL
Department of Mechanical and Aerospace Engineering, and Department of Chemical and Biochemical Engineering and Materials Science, University of California, Irvine, CA 92697 USA

An existing model of the deformation and solidification of a single droplet impinging on a cold surface has been revised and improved. The original model is based on a two-dimensional axisymmetric flow approximation of the velocity field, the Neumann solution to the one-dimensional Stefan solidification problem, and an integral mechanical energy balance. The improved model features a more appropriate velocity field which satisfies the no-shear boundary condition at the free surface, and an accurate derivation of the dissipation term from the mechanical energy equation. This equation has been solved numerically. Comparisons of the original and the improved models have been performed. Results show that the original model over-estimates the final splat size by about 10%. The discrepancy is more pronounced at larger Weber numbers, where viscous effects dominate. The effects of the Weber number, *We*, the Reynolds numbers, *Re*, and the solidification parameter have been investigated through detailed numerical calculations. Two regimes of spreading/solidification have been identified. If *Re*/*We* is small, the process is one of dissipation of the incident droplet kinetic energy; whereas for large values of *Re*/*We* the process can rather be characterized as a transfer between kinetic and potential energy. In the latter case, the variations of the final splat size versus the solidification constant exhibit a non-monotonic behaviour. This indicates that, for a given material, the deposition process can be optimized. Correlations relating the final splat size to the process parameters are given.

Nomenclature

A	area covered by the disc
b	thickness of the liquid layer
c	specific heat
D	initial droplet diameter
E_d	viscous energy dissipation
E_k	kinetic energy
E_p	potential energy
f_s	solid fraction
h_{sf}	latent heat of fusion
K	$= 6\varepsilon^2 U\rho/\rho_l(\varepsilon/Pe)^{1/2}$ solidification parameter
Pe	$= wD/\alpha$, Péclet number
Re	$= \rho_l wD/\mu$, Reynolds number
R	radius of the solid disc
r	radial coordinate
Ste	$= c(T_m - T_0)/h_{sf}$, Stefan number
T	dimensionless temperature
T_m	melting point temperature
T_0	substrate temperature
t	dimensionless time
t_c	total spreading time of the disc
U	solidification constant
V_s	volume of solidified part of the splat
V	volume of the droplet
w	impact velocity of the droplets
We	$= \rho_l Dw^2/\sigma$, Weber number
w_r	velocity component in radial direction
w_x	velocity component in axial direction
x	axial coordinate
y	solid layer thickness
α	thermal diffusivity
ε	initial disc radius to droplet diameter ratio
θ_e	contact angle of the liquid with the substrate
λ	thermal conductivity
μ	viscosity
ρ	density of the solid
ρ_l	density of the liquid
ξ	dimensionless radius of the disc
$\dot{\xi}$	$= d\xi/dt$, rate of disc expansion
σ	surface tension
$\bar{\bar{\tau}}$	viscous stress tensor
ϕ	dimensionless thickness of the liquid layer
$'$	dimensional quantity

1. Introduction

There is a variety of spray-based materials synthesis methods currently available, including low-pressure plasma deposition [1], modified gas-welding techniques [2], high-velocity oxyfuel thermal spraying [3] and spray atomization and deposition processing

0022–2461

[4]. Recently, new applications, such as self-standing structures, have attracted more attention [5]. Plasma spraying has been extensively developed as a cost-effective method of producing metallic coatings on pre-shaped parts and improving the resistance to wear and corrosion of a substrate.

There are two physical stages in a typical plasma-spraying process: (i) melting and travelling – metal powders are fed into a high-temperature plasma-flame region, melted and accelerated toward a target substrate; (ii) impact and solidification – droplets impact on the substrate and consolidate into a deposit. A significant amount of the published literature focuses on the melting and travelling stage. However, in a typical plasma-spraying process, the deformation and solidification of a single droplet plays a fairly important role. Indeed, a thorough understanding of the physical mechanisms involved in the deformation and solidification of each droplet must be acquired in order to identify the processes controlling the properties of a coating.

The general subject of liquid-drop impact on to a solid surface has been studied from a variety of points of view. A complete review of the literature has been conducted by Poulikakos and co-workers [6, 7]. The solidification of a liquid-metal drop falling on to a solid surface is a complex fluid dynamics and heat-transfer problem. When the drop impinges on the substrate, it simultaneously starts to spread and solidify. Therefore, the resulting coupled heat and momentum transfers, including phase change, occur on a time-dependent geometry. This moving boundary problem, caused by the liquid/solid interface motion, is a major issue. Mathematically, a moving boundary problem requires the solution of the governing equation in a region which has also to be determined as part of the problem. There are a few exact solutions of moving-boundary problems. For the problem considered here, the physically relevant exact solution is the solution proposed by Neumann to the Stefan solidification problem in which the thickness of the solid phase is proportional to the square root of time. This solution is used in several models [8, 9] dealing with droplet solidification to determine the thickness of the solid part of the droplet. The shortcomings of employing such a solution are described by Rangel and Bian [10, 11].

An interesting analysis of the droplet deformation and solidification process was presented by Madejski [8, 12]. This model assumes an initially spherical droplet which takes the shape of a cylindrical disc after it strikes the flat substrate. Viscous energy dissipation and surface-tension effects on the splat spreading and solidification are included. The onset of solidification is assumed simultaneous with the impact, and the Neumann solution to the Stefan one-dimensional solidification problem is adopted to solve the moving boundary problem. The motion of the spreading fluid is modelled by a mechanical energy conservation equation using a simple velocity field which satisfies only the continuity equation. Madejski's investigation yielded analytical expressions relating the final splat size to Reynolds number, the Weber number, and a solidification parameter in some special cases. No attempt was made to solve the model equation in the general case. Limited comparisons between the model's predictions and experimental data [8] show a qualitative agreement, at best.

There are two major objections to Madejski's model. First, Markworth and Saunders [13] showed that the velocity field used by Madejski does not satisfy the no-shear condition at the upper free surface, which results in a positive rate of change of viscous energy over the droplet. Markworth and Saunders [13] proposed an improved velocity field which satifies the upper surface boundary condition and correctly yields a negative integral rate of change of viscous energy. Second, the approximation used by Madejski to evaluate the viscous energy dissipation is significantly inaccurate. These deficiencies could be at the source of the discrepancies between the measured final splat size and the predicted values [8].

Furthermore, this model's assumptions are not consistent with configurations more relevant to the spray deposition processes. For instance, the possibility of nucleation prior to impact, the time lapse between impact and the start of solidification, and the possible transition to turbulent flow at high Reynolds numbers are not included in the analysis [6]. Consequently, several modifications of the Madejski model have been proposed, in order to relax some of the restricting assumptions. San Marchi *et al.* [9] investigated the effect of the partial in-flight solidification.

Bennet and Poulikakos [6] focused on the relative importance of viscous dissipation and surface tension on the maximum final splat size without solidification using the initial surface tension energy formulation proposed by Collings *et al.* [14]. However, to evaluate the energy dissipated by viscous effects, they used the expression derived by Madejski [8] based on an incorrect approximation and an unphysical velocity field [13]. These shortcomings may impair the reliability of their conclusions.

Numerical simulations of the fluid dynamics aspects of droplet spreading using the full Navier–Stokes equations, have also been conducted using finite elements [15] or finite differences [16–21]. Some of these studies [18, 21] also included solidification and yielded some insight regarding porosity formation. These more detailed approaches are more appropriate to yield a fundamental understanding of the physical processes controlling liquid-metal droplet spreading and solidification than a Madejski-type model. However, the pertinence of Madejski's model should not be overlooked. Because of its inherent simplicity, a model based on Madejski's analysis and using Markworth and Saunders' velocity field together with a proper evaluation of the viscous dissipation, has the potential to be a valuable tool in the simulation and prediction of the behaviour of the overall spray-deposition process.

It was the primary goal of the present work to build such a model. Madejski's approach was kept, but a better velocity field [13] satisfying both the continuity equation and the no-shear boundary condition at the free surface was used. A second and more

important improvement was the correct derivation of the viscous energy dissipation. Madejski expressed the viscous energy dissipation in terms of the shear stress obtained from the radial velocity gradient within the spreading splat. Here, the viscous dissipation has been carefully derived from the mechanical energy equation, assuming only negligible body force.

The resulting integro-differential equation has been solved numerically, in the general case, using a modified Euler (Predictor–Corrector) scheme. This allows an exhaustive and detailed parametric study, including the effect of the Weber and Reynolds numbers, and the solidification parameter. The temporal variation of the kinetic and potential energy and the viscous dissipation of the splat during deformation and solidification is also investigated. Previous studied [6, 8, 12] were limited to special cases where the integro-differential equation did not require numerical integration and yielded approximate analytical expressions.

2. Model

A molten metal droplet strikes on a target surface, then starts to solidify and deform (Fig. 1). At the time of impact, the droplet has a diameter D and a velocity w. The present model is based on that proposed by Madejski [8]. As shown in Fig. 2, the shape of the droplet as it impinges on the substrate is assumed to be that of a cylindrical disc. The thickness of the liquid layer is assumed uniform over the disc (independent of r), but is a function of time. The liquid layer expands radially, and the solidification begins at the time the liquid touches the substrate. The solid layer grows vertically and its thickness is a function of both t and r.

2.1. Solidification

Neumann's solution to the classical Stefan problem [22] was used. The solid front moves from the substrate towards the upper free surface of the droplet. The front position, which is the thickness of the solidified layer, y, in this model, can therefore be expressed as

$$y = U[\alpha(t' - \tau')]^{1/2} \tag{1}$$

where U is a constant depending on the Stefan number, α is the thermal diffusivity of the solid phase, and τ' is the time at which solidification begins at a given r.

As soon as the droplet touches the substrate, solidification starts and the splat radius, R, becomes larger than the initial radius, R_0, after deformation. In the region inside the initial radius $r < R_0$, $\tau' = 0$ and the thickness of the solidified layer, y_0, is only a function of time. The coordinate system used in this model is that proposed by Madejski [8] and is illustrated in Fig. 2. The initial height, $b_0 = 4R_0/3$, of the cylinder is imposed by mass conservation. The volume of the solidified layer is

$$V_s = \pi R_0^2 y_0 + \int_{\tau'=0}^{\tau'=t'} 2\pi R(\tau') y \mathrm{d}R(\tau') \tag{2}$$

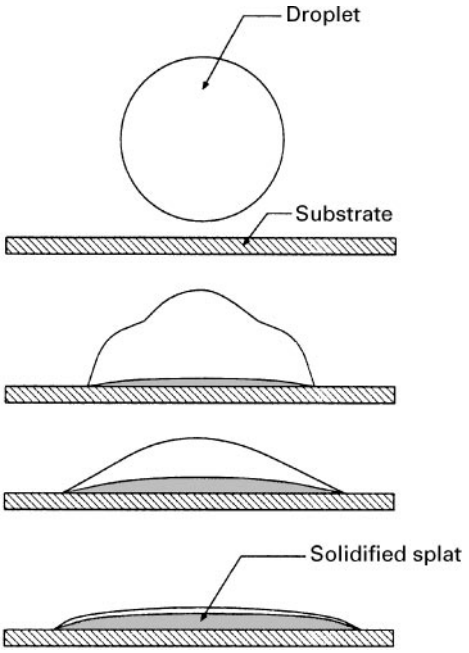

Figure 1 Schematic illustration of the problem.

Conservation of mass yields the thickness of the liquid layer as a function of time

$$b(t') = \frac{(\pi/6) D^3 \rho_l - \rho V_s}{\pi R^2 \rho_l} \tag{3}$$

2.2. Mechanical energy conservation

The liquid-disc deformation is described by the conservation of mechanical energy. The general form of the mechanical energy differential equation is [23]

$$\rho \frac{D}{Dt}\left(\frac{1}{2} w^2\right) = -(\boldsymbol{w}\cdot\nabla p) + [\boldsymbol{w}\cdot(\nabla\cdot\bar{\bar{\tau}})] + \rho(\boldsymbol{w}\cdot\boldsymbol{g}) \tag{4}$$

By assuming incompressible flow and neglecting body forces, this equation becomes

$$\frac{D}{Dt}\left(\frac{1}{2}\rho w^2\right) = \nabla(-p\boldsymbol{w} + \bar{\bar{\tau}}\cdot\boldsymbol{w}) - \bar{\bar{\tau}}:\nabla\boldsymbol{w} \tag{5}$$

Integrating over the volume of the splat and applying the divergence theorem yields

$$\underbrace{\frac{\mathrm{d}}{\mathrm{d}t}\int_V \left(\frac{1}{2}\rho w^2\right)\mathrm{d}V}_{E_k} = \underbrace{\int_A [(-p\bar{\bar{\delta}} + \bar{\bar{\tau}})\cdot\boldsymbol{w}]\cdot\hat{n}\,\mathrm{d}A}_{(I)} \underbrace{- \int_V \bar{\bar{\tau}}:\nabla\boldsymbol{w}\,\mathrm{d}V}_{\mathrm{d}E_d/\mathrm{d}t'} \tag{6a}$$

where A is the total surface area of the disc. The Leibnitz formula for differentiating a triple integral was used on the left-hand side term yielding

$$\int_V \frac{D}{Dt}\left(\frac{1}{2}\rho w^2\right)\mathrm{d}V = \frac{\mathrm{d}}{\mathrm{d}t}\int_V \left(\frac{1}{2}\rho w^2\right)\mathrm{d}V \tag{6b}$$

because the surface of the integration volume is moving with the local fluid velocity [23]. E_k is the kinetic

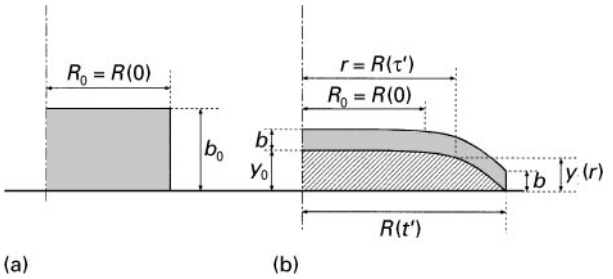

Figure 2 Coordinate system definition (after Madejski [8]). (a) $t' = 0$, (b) $t' > 0$.

energy

$$E_k = 2\pi \int_0^R \int_0^b \frac{1}{2} \rho_l (w_x^2 + w_r^2) \, dx \, r \, dr \tag{7}$$

where w_r and w_x are the radial and the axial components of the velocity field, and x is the coordinate measured perpendicular to the substrate. (I) is zero at the solid/liquid interface because of the no-slip condition. If the outside pressure is chosen as the reference pressure, the stress boundary condition on the free surface can be written [24, 25]

$$(-p\bar{\bar{\delta}} + \bar{\tau}) \cdot \hat{n} = \sigma \kappa \hat{n} \tag{8a}$$

where κ is the curvature of the free surface, $\kappa = \nabla \cdot \hat{n}$. Because only the normal components of $\bar{\tau}$ are non-zero on the free surface, $(-p\bar{\bar{\delta}} + \bar{\tau})$ is diagonal there, and

$$[(-p\bar{\bar{\delta}} + \bar{\tau}) \cdot \boldsymbol{w}] \cdot \hat{n} = [(-p\bar{\bar{\delta}} + \bar{\tau}) \cdot \hat{n}] \cdot \boldsymbol{w} = \sigma \kappa \hat{n} \cdot \boldsymbol{w} \tag{8b}$$

Therefore, after integration, (I) reduces to the rate of change of the surface tension forces on the free surface, dE_p/dt', with

$$E_p = \sigma(\pi R^2 + 2\pi R b) \tag{9}$$

Finally, the rate of viscous dissipation, dE_d/dt', is (in cylindrical coordinates)

$$\frac{dE_d}{dt'} = \int_V \mu \Phi \, dV \tag{10}$$

where

$$\Phi = \frac{\bar{\bar{\tau}} : \nabla \boldsymbol{w}}{\mu} = 2\left(\frac{\partial w_r}{\partial r}\right)^2 + 2\frac{w_r^2}{r^2} + 2\left(\frac{\partial w_x}{\partial x}\right)^2 + \left(\frac{\partial w_r}{\partial x}\right)^2 \tag{11}$$

The conservation of mechanical energy is therefore expressed as

$$\frac{d}{dt'}(E_k + E_p + E_d) = 0 \tag{12}$$

Madejski [8] approximated the viscous energy dissipation in terms of the radial shear stress and the average radial velocity within the spreading splat

$$\frac{dE_d}{dt'} = \int_0^R (2\pi r \, dr) \, \tau \boldsymbol{w}_r$$

As will be seen in Section 3.1; this equation for viscous dissipation misses an important term. Such an approach results in a reduced effect of viscous dissipation, particularly in the initial stages of the deformation.

2.3. Velocity field

The velocity field proposed by Markworth and Saunders [13] is adopted here

$$w_x = 2C'\left(\frac{x^3}{3} - bx^2\right) \tag{13a}$$

$$w_r = C' r (2xb - x^2) \tag{13b}$$

C' is a time-dependent quantity. This velocity field satisfies continuity, the no-slip condition at $x = 0$, and the boundary condition at the upper surface of the disc. The velocity field proposed by Madejski [8]

$$w_x = -Cx^2 \tag{14a}$$

$$w_r = Cxr \tag{14b}$$

satisfies continuity and the non-slip condition at the solid front, but not the boundary condition at the free surface. This is equivalent to artificially applying a shear at the upper liquid surface. With this velocity field (Equation 14a and b), the local volumetric rate of change of viscous energy, $E_v = w\mu\nabla^2 w$, is positive everywhere within the disc which means that energy is effectively being transmitted to the disc [13]. On the contrary, the velocity field proposed by Markworth and Saunders (Equation 13a and b) yields a local volumetric rate of change of viscous energy negative everywhere except in a relatively small region around the axis of symmetry.

3. Solution

3.1. Splat radius integro-differential equation

The velocity field defined above is now used to derive a workable form of the mechanical energy conservation equation. The kinetic energy expression becomes

$$E_k(t') = \frac{2}{15}\pi\rho_l C'^2 R^2 b^4 \left(R^2 b + \frac{11}{7} b^3\right) \tag{15}$$

C' can be expressed in terms of the disc expansion rate dR/dt', which is assumed equal to the average radial velocity on the splat periphery

$$C' = \frac{3}{2Rb^2}\frac{dR}{dt'} \tag{16}$$

hence

$$E_k = \frac{3}{10}\pi\rho_l \left(\frac{dR}{dt'}\right)^2 \left(R^2 b + \frac{11}{7} b^3\right) \tag{17}$$

Substituting the velocity field in the viscous dissipation equation (Equation 11) yields

$$\Phi = 12C'^2(2xb - x^2) + 4C'^2 r^2 (b - x)^2 \tag{18}$$

The viscous energy dissipation rate is obtained by integration (Equation 10)

$$\frac{dE_d}{dt'} = \frac{\pi\mu R^2}{b}\left(\frac{dR}{dt'}\right)^2\left(\frac{3}{2}+\frac{72}{5}\frac{b^2}{R^2}\right) \tag{19}$$

Evaluation of dE_d/dt' using Madejski's less-accurate expressions yields

$$\frac{dE_d}{dt'} = \frac{\pi\mu R^2}{b}\left(\frac{dR}{dt'}\right)^2 \tag{20}$$

indicating a relative error of at least 50% on the viscous dissipation rate. Bennet and Poulikakos [6] used a simplified expression based on Equation 20 to evaluate the relative effects of viscous dissipation and surface tension. Therefore, their definition of the domains, in the (Re, We) plane, where either mechanism prevails, is quantitatively inaccurate.

Equations 9, 12, 17, and 19 are then combined to yield the mechanical energy conservation equation

$$\frac{d}{dt'}\left[\frac{3}{10}\rho_l\left(\frac{dR}{dt'}\right)^2\left(R^2b+\frac{11}{7}b^3\right)+\sigma(R^2+2Rb)\right] + \frac{\mu R^2}{b}\left(\frac{dR}{dt'}\right)^2\left[\frac{3}{2}+\frac{72}{5}\frac{b^2}{R^2}\right]=0 \tag{21}$$

where the liquid thickness, b, is determined from Equation 3. Initial conditions are $R = R_0$, $b = 4R_0/3$ (from initial mass conservation), and $dR/dt'(0) = (dR/dt')_0$. The last term is deduced from the initial kinetic energy

$$E_k(0) = \frac{\pi}{6}D^3\rho_l\frac{w^2}{2} \tag{22}$$

Assuming that the initial disc radius is a fraction of initial droplet diameter, $\varepsilon = R_0/D$ the initial disc expansion can be written

$$\frac{dR}{dt'}(0) = w\left[\frac{5/3}{1+(11/252\varepsilon^6)}\right]^{1/2} \tag{23}$$

ε is determined by enforcing the conservation of the potential energy just before and just after impact

$$\pi\sigma D^2 = \sigma(\pi R_0^2 + 2\pi R_0 b_0) \tag{24}$$

Note that mass conservation imposes $b_0 = D^3/6R_0^2$. The resulting cubic has two positive real roots. The smallest root must be discarded because it corresponds to a cylinder height larger than the droplet diameter. Therefore, the only physically sound solution is $\varepsilon \simeq 0.74$. Madejski [8] inaccurately stated that it is impossible to find a value of ε satisfying the continuity of the potential energy at impact. Instead, he chose $\varepsilon = 0.5$ which, as he duly notes, yields an 8% error in the initial value of the potential energy. However, it is acknowledged that the value chosen for ε has little influence on the model. Therefore, the value of 0.5 was adopted in the present work in order to keep the comparison between Madejski's original model and the improved model as unambiguous as possible.

Finally, the equation system and the boundary conditions are normalized using R_0 as reference length and w as reference velocity. The non-dimensional variables are

$$\xi = R/R_0, \tag{25a}$$

$$\phi = b/R_0, \tag{25b}$$

$$t = wt'/R_0 \tag{25c}$$

Equations 21 and 3 become

$$\frac{d}{dt}\left[\frac{3\varepsilon}{10}\dot{\xi}^2\phi\left(\xi^2+\frac{11}{7}\phi^2\right)+\frac{\xi}{We}(\xi+2\phi)\right] + \frac{\xi^2\dot{\xi}^2}{\phi Re}\left(\frac{3}{2}+\frac{72}{5}\frac{\phi^2}{\xi^2}\right)=0 \tag{26}$$

$$\phi = \frac{1}{6\varepsilon^3\xi^2}\left\{1-K\left[\sqrt{t} + 2\int_0^t \xi(t')\dot{\xi}(t')\sqrt{(t-t')}\,dt\right]\right\} \tag{27}$$

We, Re, and Pe are the Weber, Reynolds, and Peclet numbers, and K is the solidification parameter,

$$K = 6\varepsilon^2 U\frac{\rho}{\rho_l}\left(\frac{\varepsilon}{Pe}\right)^{1/2} \tag{28}$$

The non-dimensional initial conditions for these equations are

$$\xi(0) = 1, \tag{29a}$$

$$\phi(o) = \frac{1}{6\varepsilon^3}, \tag{29b}$$

$$\dot{\xi}(0) = \left[\frac{5/3}{1+(11/252\varepsilon^6)}\right]^{1/2} \tag{29c}$$

Henceforth, Equations 26, 27, and 29a, b and c will be referred to as the improved velocity improved dissipation (IVID) model. The choice of velocity field affects the kinetic energy and dissipation terms, whereas the form of the dissipation formula affects only the dissipation term. In order to evaluate the relative effect of each modification (improved velocity field and correct viscous energy dissipation term) to Madejski's original model, three additional equation systems, similar to IVID are defined: Madejski velocity Madejski dissipation (MVMD), improved velocity Madejski dissipation (IVMD), and Madejski velocity improved dissipation (MVID). These equation systems are detailed in Table I.

3.2. Numerical solution

The dimensionless splat radius, ξ, is evaluated numerically using finite differences. First, an equation for $\dot{\xi}(t)$ is obtained by integrating the non-dimensional mechanical energy equation once from 0 to t

$$\frac{3\varepsilon}{10}\left(\frac{d\xi}{dt}\right)^2\phi\left(\xi^2+\frac{11}{7}\phi^2\right)+\frac{1}{We}\xi(\xi+2\phi) + \int_0^t\left[\xi^2\left(\frac{d\xi}{dt'}\right)^2\Big/\phi Re\right]\left(\frac{3}{2}+\frac{72}{5}\frac{\phi^2}{\xi^2}\right)dt' =$$

TABLE I Model equations and corresponding initial conditions

Model	Equation	ξ (0)	ϕ (0)	$\dot{\xi}$ (0)
MVMD	$\frac{d}{dt}\left[\frac{\varepsilon}{3}\dot{\xi}^2\phi\left(\xi^2+\frac{6}{5}\phi^2\right)+\frac{\xi}{We}(\xi+2\phi)\right]+\frac{\xi^2\dot{\xi}^2}{\phi Re}=0$	1	$\frac{1}{6\varepsilon^3}$	$\left[(3/2)\Big/\left(1+\frac{1}{30\varepsilon^6}\right)\right]^{1/2}$
IVMD	$\frac{d}{dt}\left[\frac{3\varepsilon}{10}\dot{\xi}^2\phi\left(\xi^2+\frac{11}{7}\phi^2\right)+\frac{\xi}{We}(\xi+2\phi)\right]+\frac{9}{16}\left(\frac{\xi^2\dot{\xi}^2}{\phi Re}\right)=0$	1	$\frac{1}{6\varepsilon^3}$	$\left[(5/3)\Big/\left(1+\frac{11}{252\varepsilon^6}\right)\right]^{1/2}$
MVID	$\frac{d}{dt}\left[\frac{\varepsilon}{3}\dot{\xi}^2\phi\left(\xi^2+\frac{6}{5}\phi^2\right)+\frac{\xi}{We}(\xi+2\phi)\right]+\frac{\xi^2\dot{\xi}^2}{\phi Re}\left(2+16\frac{\phi^2}{\xi^2}\right)=0$	1	$\frac{1}{6\varepsilon^3}$	$\left[(3/2)\Big/\left(1+\frac{1}{30\varepsilon^6}\right)\right]^{1/2}$
IVID	$\frac{d}{dt}\left[\frac{3\varepsilon}{10}\dot{\xi}^2\phi\left(\xi^2+\frac{11}{7}\phi^2\right)+\frac{\xi}{We}(\xi+2\phi)\right]+\frac{\xi^2\dot{\xi}^2}{\phi Re}\left(\frac{3}{2}+\frac{72}{5}\frac{\phi^2}{\xi^2}\right)=0$	1	$\frac{1}{6\varepsilon^3}$	$\left[(5/3)\Big/\left(1+\frac{11}{252\varepsilon^6}\right)\right]^{1/2}$

$$\frac{3\varepsilon}{10}\dot{\xi}^2(0)\phi(0)\left[\xi^2(0)+\frac{11}{7}\phi^2(0)\right]+\frac{1}{We}\xi(0)[\xi(0)+2\phi(0)] \quad (30)$$

After substitution of the initial conditions (Equation 29 with $\varepsilon = 0.5$), Equation 30 can be recast as

$$\dot{\xi}=\left\{\left[\frac{1}{3}\left(1+\frac{11}{We}-\frac{1}{We}\xi(\xi+2\phi)-\int_0^t\frac{\xi^2\dot{\xi}^2}{\phi Re}\left(\frac{3}{2}+\frac{72}{5}\frac{\phi^2}{\xi^2}\right)dt'\right)\Big/\left[\frac{3}{20}\phi\left(\xi^2+\frac{11}{7}\phi^2\right)\right]\right\}^{1/2}\equiv\mathscr{F}(t,\xi,\dot{\xi}) \quad (31)$$

A modified Euler predictor–corrector method is used [26]. The predictor step yields a first estimation of ξ_{n+1}, from the known value of ξ_n and $\dot{\xi}_n$ at t_n

$$\xi_{n+1}^{P}=\xi_n+\Delta t\mathscr{F}(t_n,\xi_n,\dot{\xi}_n) \quad (32)$$

Then, this estimation of ξ_{n+1} is improved using a corrector step

$$\xi_{n+1}^{C}=\xi_n+\frac{\Delta t}{2}[\mathscr{F}(t_n,\xi_n,\dot{\xi}_n)+\mathscr{F}(t_{n+1},\xi_{n+1}^{P},\dot{\xi}_{n+1}^{P})] \quad (33)$$

Because Equation 31 defines $\dot{\xi}$ implicitly, it must be solved iteratively to yield $\dot{\xi}_{n+1}$. To this end, the integral containing $\dot{\xi}$ in Equation 31 is split into two terms in order to improve the computational efficiency

$$\int_0^{t_{n+1}}\frac{\xi^2\dot{\xi}^2}{\phi Re}\left(\frac{3}{2}+\frac{72}{5}\frac{\phi^2}{\xi^2}\right)dt'=\int_0^{t_n}\frac{\xi^2\dot{\xi}^2}{\phi Re}\left(\frac{3}{2}+\frac{72}{5}\frac{\phi^2}{\xi^2}\right)dt'+\int_{t_n}^{t_{n+1}}\frac{\xi^2\dot{\xi}^2}{\phi Re}\left(\frac{3}{2}+\frac{72}{5}\frac{\phi^2}{\xi^2}\right)dt'=I_1+I_2 \quad (34)$$

Then, at any given time t_{n+1}, $\dot{\xi}_{n+1}$ can be calculated once ξ_{n+1} is known, as follows.

1. Approximate $\dot{\xi}_{n+1}$ by its previous value, $\dot{\xi}_n$.
2. Compute I_2 by the Trapezoidal rule.
3. Obtain a new $\dot{\xi}_{n+1}$ from Equation 31.
4. Repeat 2 and 3 until a desired tolerance is met.

Note that I_1 is evaluated only once during the iteration cycle. Similarly, the evaluation of ϕ_{n+1}, as defined by Equation 27, does not require knowledge of $\dot{\xi}_{n+1}$, because the integrand vanishes at t.

The obtained corrected value of ξ_{n+1} is then fed back into Equation 33 as a predicted value. Calculations showed that three corrections were sufficient.

4. Results and discussion

Three phenomena compete for the control of the spreading droplet behaviour: viscous dissipation, surface tension forces, and solidification. As a non-solidifying droplet spreads, some of its kinetic energy is transformed to potential (surface) energy while the rest is dissipated by viscous forces. Subsequently, some of the energy stored by surface tension forces may be transferred back to kinetic energy while the rest is dissipated. Thus, the edge of the splat oscillates. The oscillations stop when all the kinetic energy of the incident droplet has been dissipated by viscous forces. When solidification occurs, its effect on the final splat size depends on the relation between the solidification characteristic time and the characteristic spreading time. In most cases, solidification significantly hinders the oscillations observed in the non-solidifying case. Therefore, the model presented here was not designed to predict such oscillations. Computations are stopped when the spreading rate reaches its first zero.

4.1. Model comparison

First, the improved model (IVID) presented in the previous section is compared to Madejski's original model (MVMD). The intermediate models (IVMD and MVID) are included in this comparison in order to provide some insight into the particular effect of each modification to the original model. The reference case used for this comparison is $We = 500$, $Re = 400$, and $K = 0.02$.

All the models considered here are based on the conservation of mechanical energy (Equation 12). Fig. 3 shows the history of each term of the mechanical energy balance: kinetic energy, potential energy, and viscous dissipation during the spreading and solidification process. As the droplet spreads and solidifies, part of its initial kinetic energy is dissipated via viscous forces while the rest is stored as potential energy. In the case considered here, the potential energy remains a small fraction of the total mechanical energy of the droplet over the whole process. In fact,

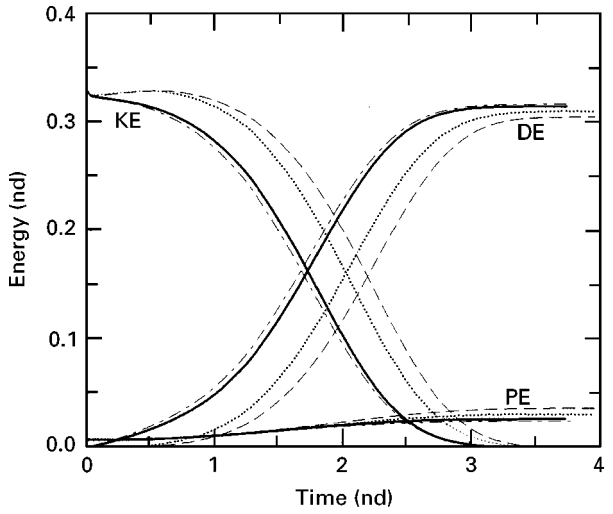

Figure 3 Comparison of the various models. Histories of kinetic (KE) and potential (PE) energies and dissipation rate (DE); nd = non-dimensional. (---) Madejski's model, (—·—) improved dissipation, (– – –) improved velocity, (——) improved dissipation and velocity.

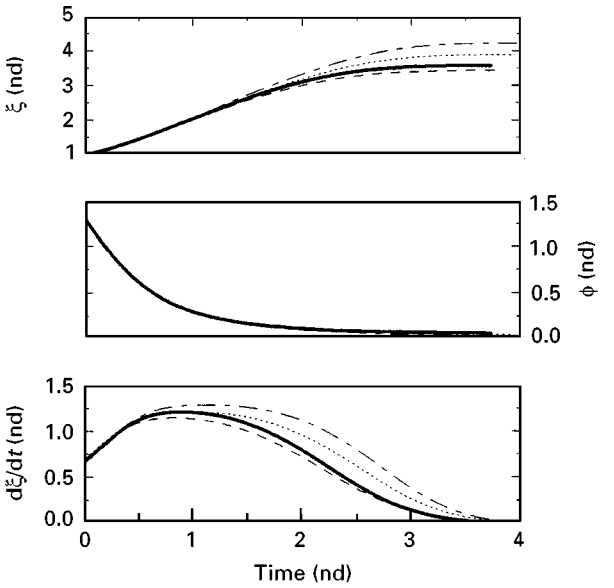

Figure 4 Comparison of the various models. Splat radius, liquid thickness, spreading rate, and solid fraction histories. (---) Madejski's model, (– – –) improved dissipation, (—·—) improved velocity, (——) improved model.

Fig. 3 shows that the droplet behaviour is dominated by the viscous dissipation of its kinetic energy.

Fig. 3 confirms that, as indicated in Section 2.2, Madejski's approach underestimates the importance of dissipation. Even more so in the initial stages of the deformation. The velocity correction (IVMD) and the dissipation modification (MVID) have opposite effects on the estimation of the dissipation rate. The improved dissipation expression yields higher dissipation rate (see also Equation 11) while Markworth and Saunders' velocity field results in a lower dissipation rate (see also Equation 18). Fig. 3 shows that, quantitatively, the dissipation modification has a more important effect than the velocity field correction because the improved model (IVID) yields a higher dissipation rate than Madejski's model. As a consequence, the improved dissipation models yield a smaller final splat size, a slightly larger final liquid thickness, and a smaller spreading rate (Fig. 4).

Madejski investigated several special cases to seek approximate analytical expressions for his original model. For completeness, the corresponding expressions have been obtained for the improved model. These correlations are listed in Table II together with Madejski's. Note that the ranges of validity of these analytical expressions are more restricted for the improved model. The case with no viscosity and no solidification ($K = 0$ and $Re^{-1} = 0$) corresponds to a reversible transfer of kinetic energy into potential energy. Therefore, the same expression is obtained with both models. In the case with no solidification and no surface tension ($K = 0$ and $We^{-1} = 0$) the relative error between the predictions of ξ_m yielded by both models is constant and equal to about 11%. For the general case without solidification, only an algebraic equation was obtained. The solutions of that equation for $100 < We < 10\,000$ and $100 < Re < 10\,000$ are plotted in Fig. 5a. At low Reynolds numbers, the final splat size is controlled by viscous dissipation and, accordingly, the plot shows almost no influence of the Weber number. For moderate to high Reynolds numbers, the spreading is surface-tension-controlled and smaller ξ_m are expected at low We. However, in this regime, the final size is reached after oscillations. As indicated above, such oscillations are not described here: computations are stopped when the spreading rate reaches its first zero. Therefore, the predicted effect of We at high Re is rather mild (Fig. 5a). The relative error between the maximum splat radius predictions of both models is plotted in Fig. 5b. At large We, the results of the case with no surface tension are recovered: the error is independent of Re and equal to about 11%. This value is the maximum error for the domain covered because the discrepancy between the model is larger at larger We, when the effects of dissipation are predominant.

TABLE II Correlations for special cases

Madejski's Model		
$K = 0$ and $Re^{-1} = 0$	$\xi_m = (We/3)^{1/2}$	for $We > 100$
$K = 0$ and $We^{-1} = 0$	$\xi_m = 1.2941 Re^{0.2}$	for $Re > 100$
$K = 0$	$3\xi_m^2/We + (\xi_m/1.2941)^5/Re = 1$	for $We > 100$ and $Re > 100$
Improved Model		
$K = 0$ and $Re^{-1} = 0$	$\xi_m \simeq (We/3)^{1/2}$	for $We > 100$
$K = 0$ and $We^{-1} = 0$	$\xi_m = 1.1626 Re^{0.2}$	for $Re > 140$
$K = 0$	$3\xi_m^2/We + (\xi_m/1.1625)^5/Re = 1$	for $We > 670$ and $Re > 140$

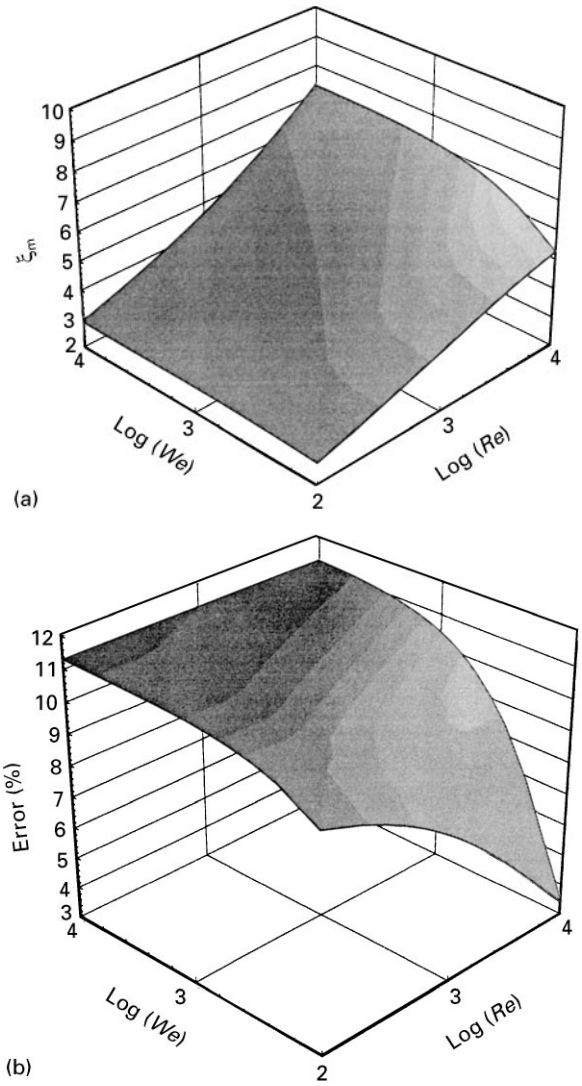

Figure 5 (a) Correlation of the final splat size with Re and We as derived from the improved model in the non-solidifying case ($K = 0$). (b) Relative error between the final splat size predicted in the non-solidifying case ($K = 0$) by Madejski's model and that obtained with the improved model.

4.2. Parametric study

An extensive parametric study was conducted, with Weber numbers ranging from 5 to 500, Reynolds numbers from 400 to 400 000, and solidification parameters from 10^{-3} to 1. These values cover the possible applications of this model as listed by Madejski [12]: thermal spraying, mist flow in boiler tubes and last stages of steam turbines, rain erosion and icing on aircrafts, and alloy splat quenching.

Intuitively, it seems clear that increasing the Weber or the Reynolds numbers, or decreasing the solidification parameter will result in a larger final splat size. This general behaviour was confirmed by Madejski's results [8, 12]. This assertion is, however, a mere description of the spreading droplet behaviour, and fails to identify the actual mechanisms controlling this behaviour. Furthermore, the influence of each parameter cannot realistically be examined independently, because their effects are closely interrelated.

Fig. 6 shows that the energy transfer history for a solidifying droplet with We of 5, 50, and 500. At low

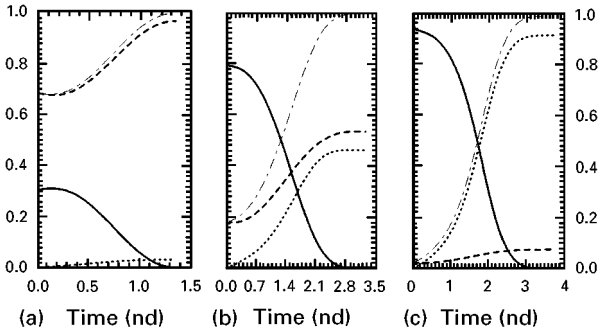

Figure 6 Energy distribution history. Effect of We ($Re = 400$ and $K = 0.02$): (a) $We = 5$, (b) $We = 50$, (c) $We = 500$. (——) KE, (---) DE, (– – –) PE, (— — —) DE + PE.

We, the potential energy is dominant, much larger than the energy dissipated by viscous forces. This case would correspond to a highly oscillatory spreading process if the droplet were not solidifying. On the contrary, at large We, dissipation dominates and the spreading would undergo negligible oscillations. The parameter defining these two regimes can be evaluated by comparing the kinetic energy per unit volume, $E_k \simeq \rho V^2/2$, the potential energy per unit volume, $E_p \simeq 6\sigma/D$, and the energy dissipated per unit volume, $E_d \simeq \mu V/D$. The ratio of the potential energy to the energy dissipated by viscous effects can be expressed as:

$$\frac{E_p}{E_d} \simeq \mathscr{A}\frac{\sigma D}{\mu V D} \simeq \mathscr{B}\frac{Re}{We} \tag{35}$$

where $\mathscr{A}$ and $\mathscr{B}$ are proportionality constants that cannot be determined through this order of magnitude analysis. If Re/We is large, the spreading process is surface-tension-dominated and oscillatory, while for small values of Re/We, most of the incident droplet kinetic energy is dissipated by viscous forces and the spreading stops with few or no oscillations. This confirms, a posteriori, the assertions made above in the interpretation of Fig. 5a.

Figs 7–9 show the influence of We, Re, or K when the two other parameters are kept constant on the history of ξ, ϕ, $\dot{\xi}$, and the solid fraction, f_s. The solid fraction of the disc is the ratio of the solid volume to the total volume. Hence (cf. Equation 3)

$$f_s = \frac{V_s}{V_s + \pi R^2 b} = 1 - \frac{3}{4}\xi^2\phi \tag{36}$$

As mentioned above, computations are stopped when the expansion rate reaches its first zero. Therefore, it is possible that, in some cases, only a small portion of the disc is solidified at the end of the computation.

Fig. 7 shows a log/linear dependence of the final splat size on the Weber number. Increasing We results in larger final splat size, smaller liquid thickness and higher final solid fraction. In all cases, the final solid

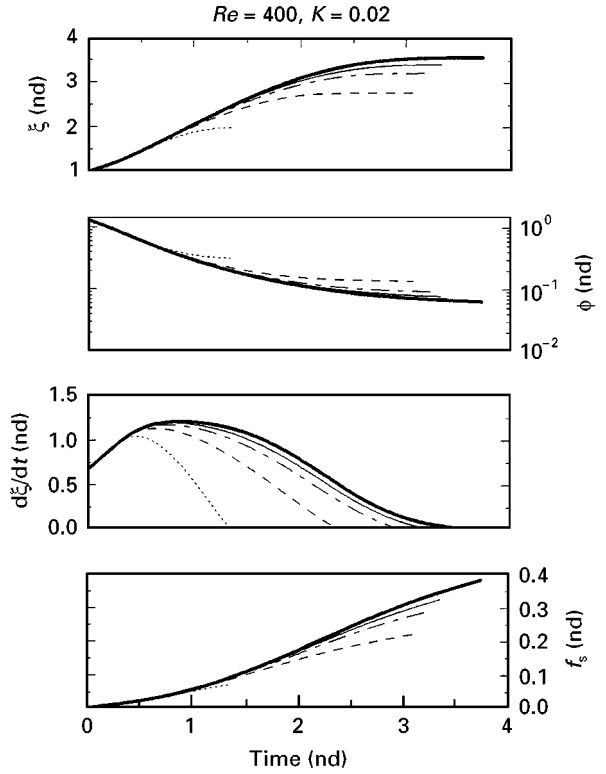

Figure 7 Splat radius, ξ, spreading rate, $\dot{\xi}$, liquid thickness, ϕ, and solid fraction, f_s, histories. Effect of the Weber number, We: (---) 5, (— — —) 20, (— - —) 50, (——) 100, (——) 500.

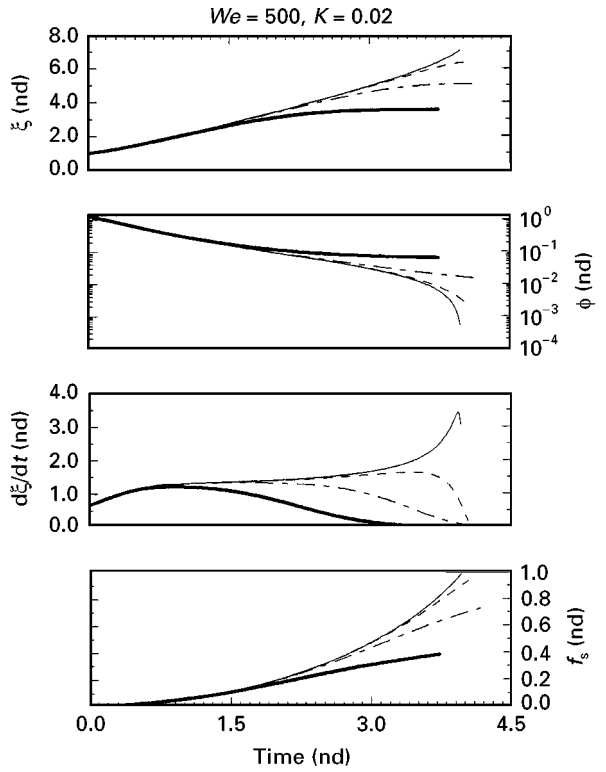

Figure 8 Splat radius, ξ, spreading rate, $\dot{\xi}$, liquid thickness, ϕ, and solid fraction, f_s, histories. Effect of the Reynolds number, Re: (——) 400, (— - —) 4000, (— — —) 40 000, (——) 400 000.

fraction is less than 0.4. The spreading stops before solidification is completed because of the relatively small value of K. At low We ($We < 50$) the spreading process is surface-tension-dominated, the spreading

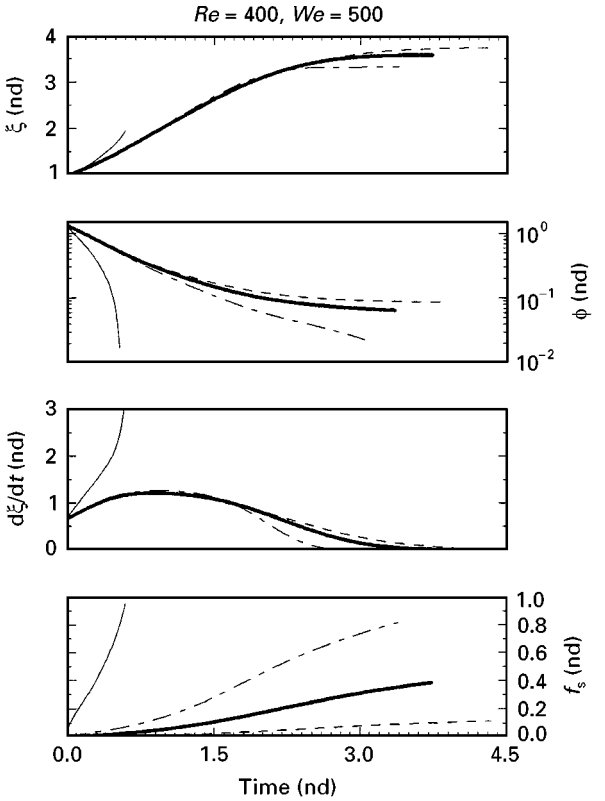

Figure 9 Splat radius, ξ, spreading rate, $\dot{\xi}$, liquid thickness, ϕ, and solid fraction, f_s, histories. Effect of the solidification parameter, K: (——) 0.5, (— - —) 0.05, (——) 0.02, (— — —) 0.005.

rate reaches zero with a finite slope thereby indicating that computations were stopped at the first extremum of ξ. At higher values of We, the spreading process is dissipation-controlled and $\dot{\xi}$ asymptotes to zero. This is consistent with the energy balances discussed above (cf. Fig. 6).

Increasing the Reynolds number also results in larger splats and higher final solid fractions (Fig. 8). In the domain covered, the final solid fraction goes from about 0.4 ($Re = 400$) to 1.0 ($Re = 400\,000$) even though K is still at 0.02. This is due to the fact that at very high Re, the splat is much thinner than at low Re and thus solidifies in a shorter time for a given value of K. At low Re, the spreading process is controlled by dissipation, and the splat asymptotes to its final size. At higher values of Re, the spreading process is surface-tension-dominated and the computations were stopped when the first extremum of ξ was reached. These results indicate the importance of the Re/We ratio on the spreading regime. For $Re = 40\,000$ and $400\,000$ (cf. Fig. 8), the expansion stops before $\dot{\xi}$ reaches zero because solidification was completed.

The solidification parameter is an indicator of the solidification speed. Varying K while keeping both Re and We constant is tantamount to investigating the influence of the Prandtl number on the spreading and solidification process. Low Prandtl numbers correspond to large values of K and thus faster solidification. Fig. 9 confirms that as K increases the liquid thickness decreases, the solid fraction increases with a final value significantly closer to unity, and the final splat size decreases. The spreading rate histories show

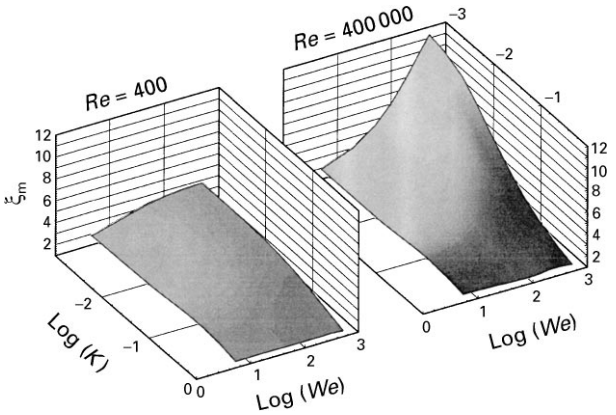

Figure 10 Final splat size parametric study. ξ_m versus We and K for $Re = 400$ and 400 000.

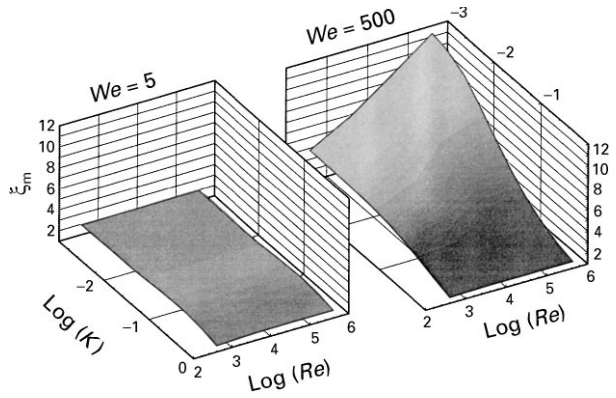

Figure 11 Final splat size parametric study. ξ_m versus Re and K for $We = 5$ and 500.

that for larger values of K the solidification process controls the final splat size.

Figs 10–12 focus on the combined effects of We, Re and K on the final splat size. Both Figs 10 and 11 corroborate the previously established significance of the Re/We ratio in determining the spreading regime. There is a significant effect of We (or respectively Re) on the final splat size only for higher values of Re (or respectively We), when the spreading process is surface-tension (or respectively dissipation)-controlled. These two figures also show how the spreading process is affected by solidification. Higher values of K substantially reduce the effect of We (or respecitvely Re) on the final splat size at high Re (or respectively We).

Another feature of interest illustrated by Figs 10 and 11 is the non-monotonic behaviour of the final splat size versus K at low We ($We < 50$) for all values of Re. For $We = 5$, ξ_m is nearly constant for small values of K up to about 0.02, then increases and reaches a maximum for $K \simeq 0.2$, and finally decreases. This is unexpected because higher values of K (faster solidification) yield smaller final splat size in all other cases. This feature is better seen in Fig. 12. It was demonstrated in the previous paragraphs that at such small Weber numbers the spreading process is surface-tension-controlled (see also Fig. 6). For very small values of K solidification has a negligible influence and the final splat size is determined by the value of

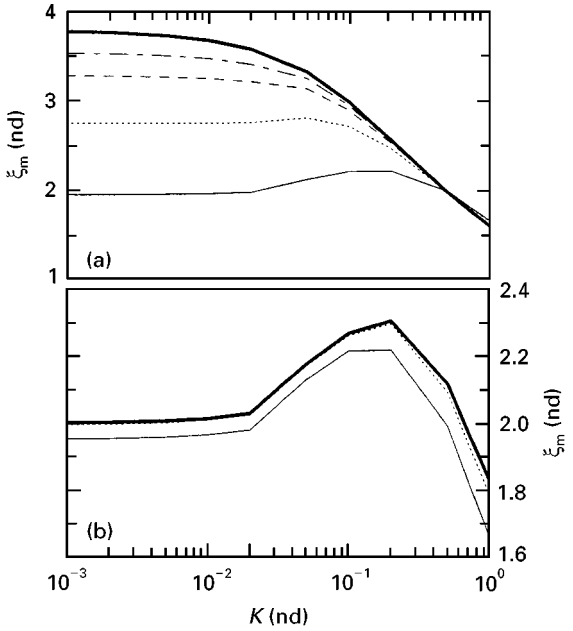

Figure 12 Final splat size non-monotonic behaviour at low We: (a) $Re = 400$, We: (——) 5, (---) 20, (– – –) 50, (— - —) 100, (——) 500. (b) $We = 5$, Re: (——) 4×10^2, (---) 4×10^3, (– – –) 4×10^4, (——) 4×10^5.

We only. As K increases, the liquid mass decreases thus causing the liquid velocity to increase in order to conserve kinetic energy. This mechanism enhances the spreading process, resulting in a larger final splat size. In this phase, solidification becomes less negligible but still does not control the final splat size. This trend is reversed when K is large enough to directly control the final splat size. Note that the values of K delimiting this behaviour depend on We.

4.3. Some practical examples

The results presented above show that the effects of Re, We, and K on droplet spreading and solidification should not be evaluated separately. Indeed, in practical cases, the values of Re, We and K cannot be varied independently. Two practically relevant questions can be formulated. How do the operating conditions (droplet size, temperature, and impact velocity) affect the final splat size for a given metal, and how does the final splat size change when, for given operating conditions, the metal is changed? In order to provide limited answers to these questions, the present model was applied to the cases of various metals: Aluminium ($T_{mp} = 933$ K), titanium ($T_{mp} = 1958$ K), nickel ($T_{mp} = 1727$ K), copper ($T_{mp} = 1356$ K), and tungsten ($T_{mp} = 3650$ K). The corresponding properties are listed in Table III. The operating conditions considered include liquid temperatures at the melting point and 100 K above the melting point, initial velocities of 1, 10 and 100 m s^{-1} and initial disc diameters of 0.1, 1, and 10 mm. The substrate is at room temperature (300 K). The solidification constant, U, was calculated for each metal and temperature.

For a given metal, the effect of a droplet size or impact velocity increase is consistent with the resulting

TABLE III Metal properties used

	T_{mp}			T_{mp} + 100 K		
	ρ (kg m^{-3})	σ (N m^{-1})	μ (kg m^{-1} s^{-1})	ρ (kg m^{-3})	σ (N m^{-1})	μ (kg m^{-1} s^{-1})
Al	2385	0.914	1.50×10^{-4}	2357	0.879	1.50×10^{-4}
Ti	4110	1.650	5.20×10^{-3}	4040	1.624	5.20×10^{-3}
Ni	7905	1.778	1.67×10^{-4}	7789	1.740	1.67×10^{-4}
Cu	8000	1.285	3.02×10^{-4}	7920	1.272	3.02×10^{-4}
W	17600	2.500	3.00×10^{-3}	17450	2.471	3.00×10^{-3}

TABLE IV Final disc diameter (mm) for selected metals: aluminium (T_{mp} = 933 K), titanium (T_{mp} = 1958 K), nickel (T_{mp} = 1727 K), copper (T_{mp} = 1356 K), tungsten (T_{mp} = 3650 K). The substrate is at 300 K.

			Final disc diameter (mm)				
	D (mm)	V (m s^{-1})	Al	Cu	W	Ni	Ti
T_{mp}	0.1	1	0.1438	0.1639	0.1550	0.1665	0.1767
		10	0.1748	0.1685	0.1820	0.1987	0.2145
		100	0.2558	0.2626	0.2880	0.3133	0.3411
	1	1	1.7166	1.7889	1.9280	2.0619	2.0618
		10	2.5579	2.6234	2.8730	3.1075	3.3727
		100	4.0979	4.3209	4.5130	4.9589	5.3911
	10	1	25.412	25.992	28.005	30.648	31.467
		10	40.585	42.968	45.006	49.302	53.910
		100	63.836	65.520	71.258	79.365	85.390
T_{mp} + 100 K	0.1	1	0.1481	0.1443	0.1460	0.1693	0.1772
		10	0.1749	0.1849	0.1860	0.2087	0.2206
		100	0.2719	0.2935	0.2900	0.3240	0.3499
	1	1	1.8036	1.8624	1.9220	2.0683	2.0650
		10	2.7079	2.9177	2.8950	3.2079	3.4805
		100	4.3072	4.5498	10.278	5.2246	5.5335
	10	1	26.127	28.013	29.25	32.444	31.996
		10	42.668	45.062	45.745	52.214	55.291
		100	67.286	72.172	70.525	82.240	87.571

increases of both Re and We, and decrease of K: a larger final splat is obtained (cf. Table IV). Increasing the liquid temperature results in lower values of U and thus of K which, in turn, yields slightly larger final splats.

The results also show that titanium yields the largest final splat size under most conditions (cf. Table IV). Titanium has a much larger (kinematic) viscosity than the other metals considered here (one to two orders of magnitude), and its surface tension coefficient is average (cf. Table III). Therefore, one would expect titanium to yield smaller splat sizes than the other metals, at given operating conditions. However, the thermal diffusivity of titanium is almost one order of magnitude smaller than that of the other metals (cf. Table III) which causes the corresponding value of the solidification parameter, K, to be smaller for titanium in all cases considered (the value of U does not vary significantly for the metals and temperatures considered, the average value is about 1.6). These results show the predominance of solidification on the value of the final splat size.

5. Conclusion

The model proposed by Madejski [8] for the spreading and solidification of a liquid metal droplet impinging on a flat surface has been improved. Markworth and Saunders' velocity field was used, thus providing a more accurate evaluation of the shear stress field [13]. Viscous dissipation was derived from the mechanical energy equation rather than using Madejski's assumption.

The improved model predicts a smaller ($\approx 10\%$) final splat size than the original model. The discrepancy is more pronounced at larger Weber numbers, where viscous effects dominate. A detailed parametric study permitted the identification of two regimes of spreading/solidification delimited by the Reynolds to Weber ratio. For small values of Re/We ($Re/We < 8$), the process is controlled by dissipation; whereas for large values of Re/We ($Re/We > 8$) the process surface tension dominates. In both cases solidification takes over for large values ($K > 0.1$) of the solidification parameter. The final splat size is therefore determined by the value of Re/We and that of K. For

small Weber numbers (below 20), the variations of the final splat size versus the solidification constant exhibit a non-monotonic behaviour. This indicates that, for a given material, the deposition process can be optimized.

Acknowledgements

This work was sponsored in part by Sulzer Metco (Irvine) Inc. and by NSF (CTS 92-24850). This research was also supported in part by the University of California, Irvine through an allocation of computer resources. The authors thank Ms Lisa Kuo for performing the numerical computations.

References

1. D. WEI, B. FROUK and D. APELIAN, in "Plasma Processing and Synthesis of Materials", edited by J. Szekely and D. Apelian (Materials Research Society, Pittsburgh, PA, 1987).
2. W. LUCAS, "TIG and Plasma Welding-Process Techniques, Recommended Practices and Applications" (Abington, Cambridge, 1990).
3. Flame Coatings PIY Ltd, Sydney, Australia, "Superiors/HVOF Coatings-Higher Particle Velocities Produce Better Thermal Spray Coatings", Internal Report.
4. X. ZENG, H. LIU, M. CHU and E. J. LAVERNIA, *Metall. Trans. B Process Metall.* **23A** (1992) 3394.
5. R. TIWARI, H. HERMAN, S. SAMPATH and B. GUDMUNDSSON, *Mater. Sci. Eng. A Struct. Mater. Prop. Microstruct. Process.* **144** (1991) 127.
6. T. BENNETT and D. POULIKAKOS, *J. Mater. Sci.* **28** (1993) 963.
7. D. POULIKAKOS and J. WALDVOGEL, "Transport phenomena relevant to the impact regime of the process of spray deposition; a review", presented at the 24th National Heat Transfer Conference, Heat Transfer division of the ASME Portland. OR, 5–9 August 1995.
8. J. MADEJSKI, *Int. J. Heat Mass Transfer* **19** (1976) 1009.
9. C. SAN MARCHI, H. LIU, E. J. LAVERNIA and R. H. RANGEL, *J. Mater. Sci.* **28** (1993) 3313.
10. R. H. RANGEL and X. BIAN, *Int. J. Heat Mass Transfer* **39** (1995) 1591.
11. *Idem*, *Numerical Heat Transfer, A Applications* **28** (1995) 589.
12. J. MADEJSKI, *Int. J. Heat Mass Transfer*. **26** (1983) 1095.
13. A. J. MARKWORTH and J. H. SAUNDERS, *ibid.* **35** (1992) 1836.
14. E. COLLINGS, A. MARKWORTH, J. McCOY and J. SAUNDERS, *J. Mater. Sci.* **25** (1990) 3677.
15. J. FUKAI, Z. ZHAO, D. POULIKAKOS, C. M. MEGARIDIS and O. MIYATAKE, *Phys. Fluids* **5** (1993) 2588.
16. G. TRAPAGA and J. SZEKELY, *Metall. Trans. B Process Metall.* **22B** (1991) 901.
17. G. TRAPAGA, E. F. MATTHYS, J. J. VALENCIA and J. SZEKELY, *ibid.* **23B** (1992) 70.
18. H. LIU, E. J. LAVERNIA and R. H. RANGEL, *Atomiz. Sprays* **4** (1994) 369.
19. *Idem*, *J. Thermal Spray Technol.* **2** (1993) 369.
20. *Idem*, *Acta Metall. Mater.* **43** (1995) 2053.
21. J.-P. DELPLANQUE, E. J. LAVERNIA and R. H. RANGEL, *Numerical Heat Transfer* A **30** (1996) 1.
22. M. OZISIK, "Heat Conduction" (Wiley, New York, 1980).
23. R. B. BIRD, W. E. STEWART and E. W. LIGHTFOOT, "Transport phenomena" (Wiley, New York, 1980).
24. L. D. LANDAU and E. M. LIFSHITZ, "Fluid Mechanics" (Pergamon Press, New York, 1959).
25. L. G. LEAL, "Laminar flow and convective transport processes – Scaling principles and asymptotic analysis" (Butterworth-Heinemann, Boston, 1992).
26. J. D. HOFFMAN, "Numerical Methods for Engineers and Scientists" (McGraw-Hill, New York, 1992).

Received 4 December 1995
and accepted 8 May 1996